EPRI | ELECTRIC POWER RESEARCH INSTITUTE

Program on Technology Innovation: Spatial Coherency Models for Soil-Structure Interaction

1012968

Program on Technology Innovation: Spatial Coherency Models for Soil-Structure Interaction

1012968

Technical Update, January 2006

EPRI Project Managers

R. Kassawara
L. Sandell

Cosponsor

U.S. Department of Energy
Office of Nuclear Energy
Sciences and Technology
19901 Germantown Road, NE-20
Germantown, MD 20874-1290

ELECTRIC POWER RESEARCH INSTITUTE
3420 Hillview Avenue, Palo Alto, California 94304-1395 • PO Box 10412, Palo Alto, California 94303-0813 • USA
800.313.3774 • 650.855.2121 • askepri@epri.com • www.epri.com

DISCLAIMER OF WARRANTIES AND LIMITATION OF LIABILITIES

ORGANIZATION(S) THAT PREPARED THIS DOCUMENT

Norman A. Abrahamson, Inc.

This is an EPRI Technical Update report. A Technical Update report is intended as an informal report of continuing research, a meeting, or a topical study. It is not a final EPRI technical report.

NOTE

For further information about EPRI, call the EPRI Customer Assistance Center at (800) 313-3774 or email askepri@epri.com.

CITATIONS

This report was prepared by

Norman A. Abrahamson, Inc.
152 Dracena Avenue
Piedmont, CA 94611

Principal Investigator
N. Abrahamson

This document describes research sponsored by the Electric Power Research Institute (EPRI) and the U.S. Department of Energy under Award No. (DE-FC07-04ID14533). Any opinions, findings, and conclusions or recommendations expressed in this material are those of the author(s) and do not necessarily reflect the views of the Department of Energy.

The report is a corporate document that should be cited in the literature in the following manner:

Program on Technology Innovation: Spatial Coherency Models for Soil-Structure Interaction. EPRI, Palo Alto, CA, and U.S. Department of Energy, Washington, DC: 2006. 1012968.

ABSTRACT

The spatial incoherency of strong ground motions has the effect of reducing the response of building foundations to the high frequency portion of these motions. Strong ground motion recordings show earthquake response motions at building foundations to be less intense than corresponding free-field motions. To fully explain this difference as part of soil-structure interaction (SSI) effects, it is necessary to consider spatial variations in free-field motions within the building foundation footprint. This study reviews current coherency models developed from work at the Lotung large-scale seismic test (LSST) facility and from seismic studies for the major toll bridges in California. The models are modified for application to SSI analyses for nuclear power plants, and the data sets used to derive them are briefly described.

CONTENTS

LIST OF FIGURES

LIST OF TABLES

1
INTRODUCTION

An overview of spatial coherency studies is given by Zerva, A. and V. Zervas (2002). Most of the studies of spatial coherency are based on evaluation of the ground motions from the dense array located in Lotung Taiwan due to the extensive database that is available from the SMART 1 array. The SMART-1 array has station spacing of 100-4000m (Abrahamson et. al. 1987). Using data from the SMART-1 array, coherency models have been developed by several authors: Abrahamson, (1993), Harichandran and Vanmarcke (1986), Harichandran (1988), Harichandran (1991), Loh (1985), Loh and Yeh (1988), Loh and Lin (1990), Novak (1987), Oliveira et. al. (1991), Ramadan and Novak (1993), Vernon et al. (1991), and Zerva and Zhang (1997). Given the dimensions of the SMART-1 array, these studies have been focused on coherency for station separations that are greater than foundation sizes for nuclear power plants.

To address the spatial variation over dimensions of foundations for nuclear power plants, EPRI supported the installation of the EPRI LSST array, also located in Lotung, Taiwan. The EPRI LSST array is described in Abrahamson et. al. (1991) and has station spacings of 3 - 85 m. The spatial coherency from the denser EPRI LSST array data was studied by Abrahamson and Schneider (1988) and Abrahamson et. al. (1991).

With the SMART-1 and LSST array data, we have well calibrated empirical models for the coherency in Lotung, Taiwan. A key question is: are the coherency models from Lotung, Taiwan applicable to other regions? This question was addressed by Abrahamson et. al. (1992). They compared the coherency models developed using the LSST array data with coherency measured from dense arrays in other regions. They found that, other than for sites with strong topography, there is not a significant dependence of the coherency on the site condition or earthquake magnitude.

A coherency model using both the SMART-1 and LSST data, as well as data from ten other dense arrays, was developed by Abrahamson (1998). This model covers station separations distances of 6-4000m. It was developed as part of the seismic studies for the major toll bridges in California and is only described in an appendix to a report to Caltrans. This Caltrans appendix gives the equation for the coherency model but does not include a description of how the model was derived.

The objective of this study was to review the current coherency models and make any modifications needed for application to SSI analyses for nuclear power plants. In addition, a brief description of the data sets used to derive the coherency model is included.

2
MATHEMATICAL BACKGROUND

The spatial variability of the ground motion waveforms can be quantified by the spatial coherency. Let $u_j(\omega)$ be the Fourier transform of the tapered time series $u_j(t)$, then

$$u_j(\omega) = \sum_{k=1}^{T} v(t_k) u_j(t_k) \exp(-i\omega t_k) \qquad \textbf{(Equation 2-1)}$$

where $v(t_k)$ is the data taper, T is the number of time samples, t_k is the time of the k^{th} sample, and ω is the frequency. The smoothed cross-spectrum is given by

$$S_{jk}(\omega) = \sum_{m=-M}^{M} a_m u_j(\omega_m) \overline{u}_k(\omega_m) \qquad \textbf{(Equation 2-2)}$$

where 2M+1 is the number of discrete frequencies smoothed, $\omega_m = \omega + 2\pi m/T$, a_m are the weights used in the frequency smoothing, and the overbar indicates the complex conjugate. The coherency, $\gamma_{ij}(\omega)$, is given by

$$\gamma_{ij}(\omega) = \frac{S_{ij}(\omega)}{S_{ii}(\omega) S_{jj}(\omega)} \qquad \textbf{(Equation 2-3)}$$

where $S_{ij}(\omega)$ is the smoothed cross-spectrum for stations i and j. As shown in Eq. 2-3, the coherency is a complex number. It is common to use the absolute value of the coherency (sometimes called the lagged coherency because it lags the data to remove the wave-passage effect). A $Tanh^{-1}$ transformation is applied to the lagged coherency to produce approximately normally distributed data (Enochson and Goodman, 1965). That is, the $Tanh^{-1}$ ($|\gamma|$) will be approximately normally distributed about the median $Tanh^{-1}(|\gamma|)$ curve. This is a well-known transformation used in time series analysis.

The computed lagged coherency depends strongly on the selected frequency smoothing. If no smoothing is used, then the lagged coherency is always unity. In this evaluation of coherency, an 11-point Hamming window is used for the frequency smoothing (a_m) and a 5% double cosine bell taper is used for the data window (v(t)). (This means that the complex cross spectrum in Eq. 2-2 is averaged over 11 frequencies using weights that are close to a triangle weighting scheme). In order to make consistent comparisons of lagged coherency for different earthquakes, it is important to keep the number of discrete frequencies smoothed fixed. This can lead to different frequency bands for the frequency smoothing if the window lengths are not the same for all events.

There are several ways the coherency can be described: lagged coherency, plane-wave coherency, and unlagged coherency. These three measures of coherency are described below.

The lagged coherency is the most commonly cited coherency measure. It is the coherency measured after aligning the time series using the time lag that leads to the largest modulus of the cross spectrum. It is given by $|\gamma|$. There is no requirement that the time lags are consistent between frequencies. In general, the lagged coherency does not go to zero at large separations and high frequencies. The level depends on the number of frequencies smoothed.

The plane-wave coherency differs from the lagged coherency in that it uses a single time lag for all frequencies. That is, it measures the coherency relative to a single wave speed for each earthquake. As a result, the plane-wave coherency is smaller than the unlagged coherency. The plane-wave coherency is found by taking the real part of the smoothed cross-spectrum after aligning the ground motions on the best plane-wave speed. The plane–wave coherency will approach zero at high frequencies and large separations.

Finally, the unlagged coherency measures the coherency assuming no time lag between locations. It is the real part of the smoothed cross-spectrum. The unlagged coherency will be smaller than the plane-wave coherency. The unlagged coherency is found by multiplying the plane-wave coherency by $\cos(2\pi f \xi_R s)$ where f is the frequency, ξ_R is the separation distance in the direction of wave propagation, and s is the wave slowness (inverse of the apparent velocity). The coherent part of the wave passage effect can lead to negative values of the unlagged coherency.

3
COHERENCY MODELS

To evaluate the effects of spatial coherency for large foundations requires a coherency function defined for short station separations (e.g. 0-200 m). Abrahamson et. al. (1991) developed coherency functions based on the EPRI LSST array data, which is a dense array located on a soil site in Taiwan. The LSST array included data recorded from magnitudes between 3.0 and 7.8. They found that there was no dependence of the coherency on the earthquake magnitude.

Since the LSST array was located on soil, there was a question regarding the applicability of this model to rock sites. Abrahamson and Schneider (1992) compared the lagged coherency model from the LSST array with coherencies computed from nine other arrays located on rock and soil site conditions. The dense arrays considered in this comparison are listed in Table 3-1. The earthquakes from the dense arrays are summarized in Table 3-2. The lengths of the time windows used to estimate the coherency are listed in Table 3-3. These time windows range from 2.0 to 10 seconds with most of the window lengths of about 5 seconds. These window lengths were chosen to capture the strongest shaking on the horizontal component (e.g., S-wave window). The coherency is measured over the specified window lengths.

Abrahamson et. al. (1992) compared the coherencies from the arrays listed in Table 3-1 with the Abrahamson et. al. (1991) LSST based coherency model and fund that, overall, there is no systematic difference between the lagged coherencies on rock and soil sites, but rock site arrays with strong topographic differences showed lower coherencies than the LSST model.

In developing the Abrahamson (1998) coherency model, the data from the USGS Parkfield and UCSC ZAYA arrays were not included because the low coherencies observed at these arrays could be due to topographic effects. Using the data from the ten remaining arrays (two large arrays and eight dense arrays), new coherency models were developed. As in the LSST study, the coherency was fit to the $\text{Tanh}^{-1}(|\gamma|)$; however, the final model for the plane-wave coherency was presented in terms of the coherency. This was done because it allowed the final model to be constrained to yield unit coherency at zero separation distance and zero frequency.

Table 3-1
Arrays Used to Develop the Coherency Models

Array	Location	Site Class	Topography	Number of Stations	Station Separation (m)
EPRI LSST	Taiwan	Soil	Flat	15	3 – 85
EPRI Parkfield	CA	Soft Rock	Flat	13	10 – 191
Chiba	Japan	Soil	Flat	15	5 – 319
USGS Parkfield	CA	Soft Rock	Ridge Tops	14	25 – 952
Imperial Valley Differential	CA	Soil	Flat	5	18 – 213
Hollister Differential	CA	Soil	Flat	4	61 – 256
Stanford (Temp)	CA	Soil	Flat	4	32 – 185
Coalinga (Temp)	CA	Soft-Rock	Flat	7	48 – 313
UCSC ZIYA (Temp)	CA	Soft-Rock	Mountains	6	25 – 300
Pinyon Flat (Temp)	CA	Hard-Rock	Flat	58	7 – 340
SMART-1	Taiwan	Soil	Flat	39	100 – 4,000
SMART-2	Taiwan	Soil	Flat	8	200 - 750

Table 3-2
Earthquakes in the Array Data Sets

Array	No. of Earthquakes	Magnitudes	Rupture Distances (km)	Maximum PGA (g)
EPRI LSST	15	3.0 – 7.8	5-113	0.26
EPRI Parkfield	2	3.0 – 3.9	13-15	0.04
Chiba	9	4.8 – 6.7	61-105	0.41
USGS Parkfield	9	2.2 – 3.5	18-45	0.04
Imperial Valley Differential	2	5.1 – 6.5		0.89
Hollister Differential	1	5.3	17	0.20
Stanford (Temp)	4	3.0 – 4.0	40	0.007
Coalinga (Temp)	1	5.2	12	0.21
UCSC ZIYA (Temp)	3	2.3 – 3.0	9-19	
Pinyon Flat (Temp)	6	2.0 – 3.6	14-39	
SMART-1	20	4.0 – 7.8	5-80	0.33
SMART-2	2	4.0 – 5.5	15-60	0.06

Table 3-3
Window Lengths (in sec) Used in the Coherency Estimates from Dense Arrays

Array Name	Earthquake Number														
	1	2	3	4	5	6	7	8	9	10	11	12	14	16	17
Chiba	5.0	5.0	5.0	5.0	4.5	5.0	4.5	5.0	5.0						
EPRI LSST		3.5	5.0	5.0	2.5	5.0	5.0	5.0		2.5	2.5	5.0	2.5	10	10
EPRI Parkfield	2.0	2.5													
Hollister	5.0														
Imperial Valley	5.0	5.0													
Pinyon Flat	2.5	2.5	2.5	2.5	2.5	2.5									
Coalinga	2.0	2.0	2.0	2.0	2.0	2.0	2.0								
USGS Parkfield	5.0		5.0	5.0	5.0	5.0	4.0	5.0	5.0	5.0					
UCSC ZAYA	5.0	5.0	5.0												
Stanford	4.0	5.0	5.0	4.5											

The Abrahamson (1998) model was modified to require coherency=1 for separation distances of 0 by adding the Tanh($a_3\xi$) term. The data do not provide a constraint for separation distances less than 6 m; the 3 m separations from the LSST data are excluded because they are affected by SSI. As a result, the a_3 value was simply selected to give a smooth transition to unity at zero distance. Tests using alternative values of a_3 showed that the SSI is not sensitive to the choice of a_3. The equations for the modified model are given below:

$$\gamma_{pw}(f,\xi)=\left[1+\left(\frac{f\ \ Tanh(a_3\xi)}{a_1 f_c(\xi)}\right)^{n1}\right]^{-1/2}\left[1+\left(\frac{f\ \ Tanh(a_3\xi)}{a_2 f_c(\xi)}\right)^{n2(\xi)}\right]^{-1/2} \qquad \textbf{(Equation 3-1)}$$

$$\gamma_{UN}(f,\xi)=\left|\gamma_{pw}(f,\xi)\right|\cos(2\pi f\xi_R s) \qquad \textbf{(Equation 3-2)}$$

$$\gamma\,(f,\xi)=\left|\gamma_{pw}(f,\xi)\right|\left(\cos(2\pi f\xi_R s)+i\sin(2\pi f\xi_R s)\right) \qquad \textbf{(Equation 3-3)}$$

where f is the frequency in Hz, ξ is the separation distance in m, s is the slowness in s/m and ξ_R is the separation distance in the radial direction in m, The coefficients for the model are given in Tables 3-4 and 3-5 for the horizontal and vertical components. Eq. 3-1 gives the plane-wave coherency, which should be used if a single inclined wave is used as the input to the SSI model. Eq. 3-2 gives the unlagged coherency, which should be used if a vertically inclined wave is used in the SSI. The complex coherency in Eq. 3-3 can be used with vertically inclined waves to capture the systematic phase shifts due to an inclined wave. The ξ_R term in Eqs. 3-2 and 3-3 depend on the direction of the wave propagation. For a generic application, the median value of ξ_R will be

$$\xi_r=\frac{\xi}{\sqrt{2}} \qquad \textbf{(Equation 3-4)}$$

The imaginary term will depend on the direction of the wave-propagation (e.g., positive or negative slowness). Its median value will be zero for a random wave direction, but for each earthquake, it will be non-zero.

Table 3-4
Plane-Wave Coherency Model Coefficients for the Horizontal Component

Coeff	Horizontal Component
a_1	1.647
a_2	1.01
a_3	0.4
n_1	7.02
$n_2(\xi)$	5.1 - 0.51 ln(ξ+10)
$f_c(\xi)$	$f_c(\xi) = -1.886 + 2.221 \ln\left(\frac{4000}{\xi+1} + 1.5\right)$
s	0.0005 s/m to 0.00025 s/m

Table 3-5
Plane-Wave Coherency Model Coefficients for the Vertical Component

Coeff	Vertical Component
a_1	3.15
a_2	1.0
a_3	0.4
n_1	4.95
$n_2(\xi)$	1.685
$f_c(\xi)$	$f_c(\xi) = \exp\left(2.43 - 0.025\ln(\xi+1) - 0.048[\ln(\xi+1)]^2\right)$
s	0.0005 s/m to 0.00025 s/m

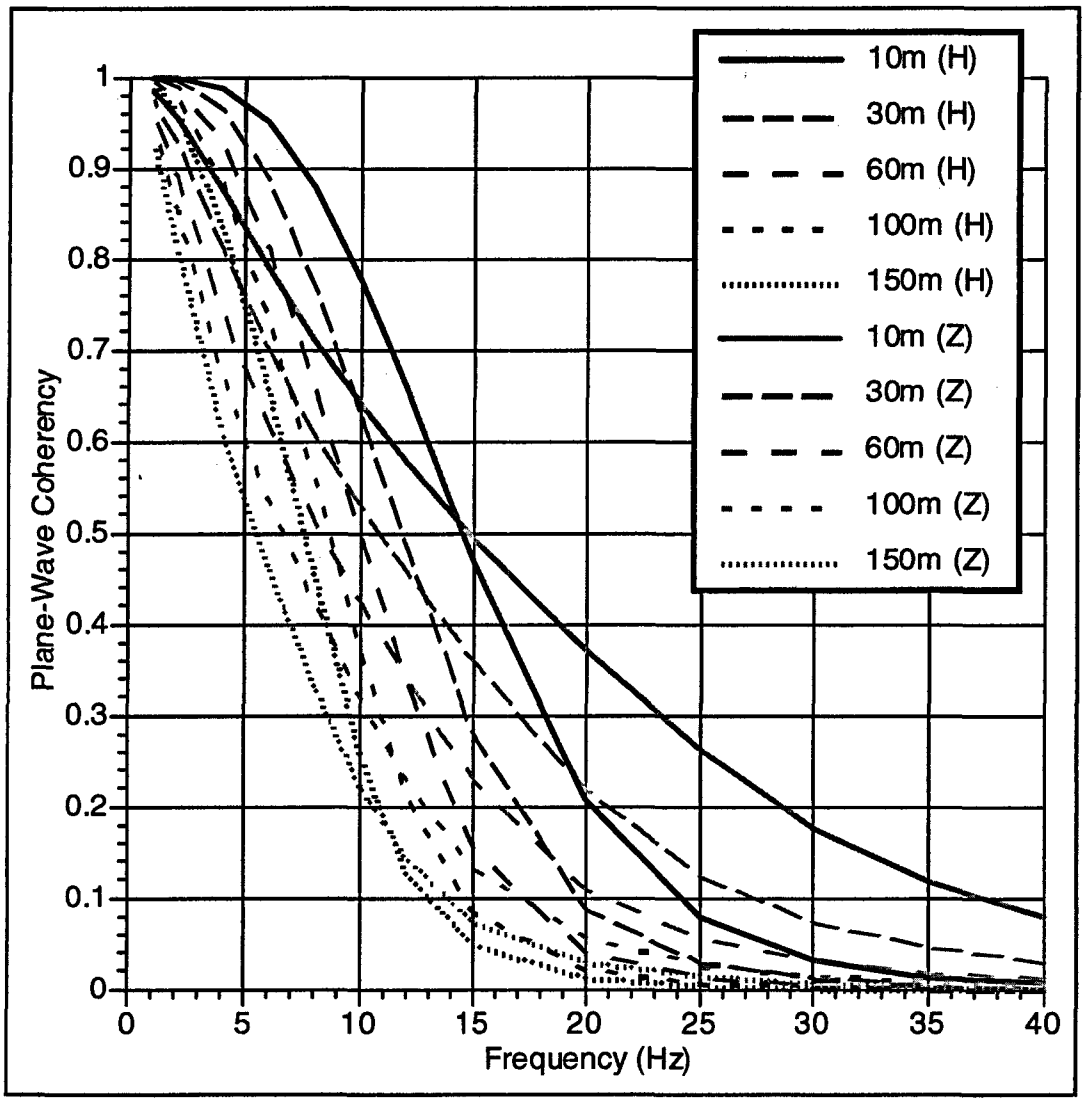

Figure 3-1
Comparison of the Horizontal and Vertical Component Plane-Wave Coherency Models

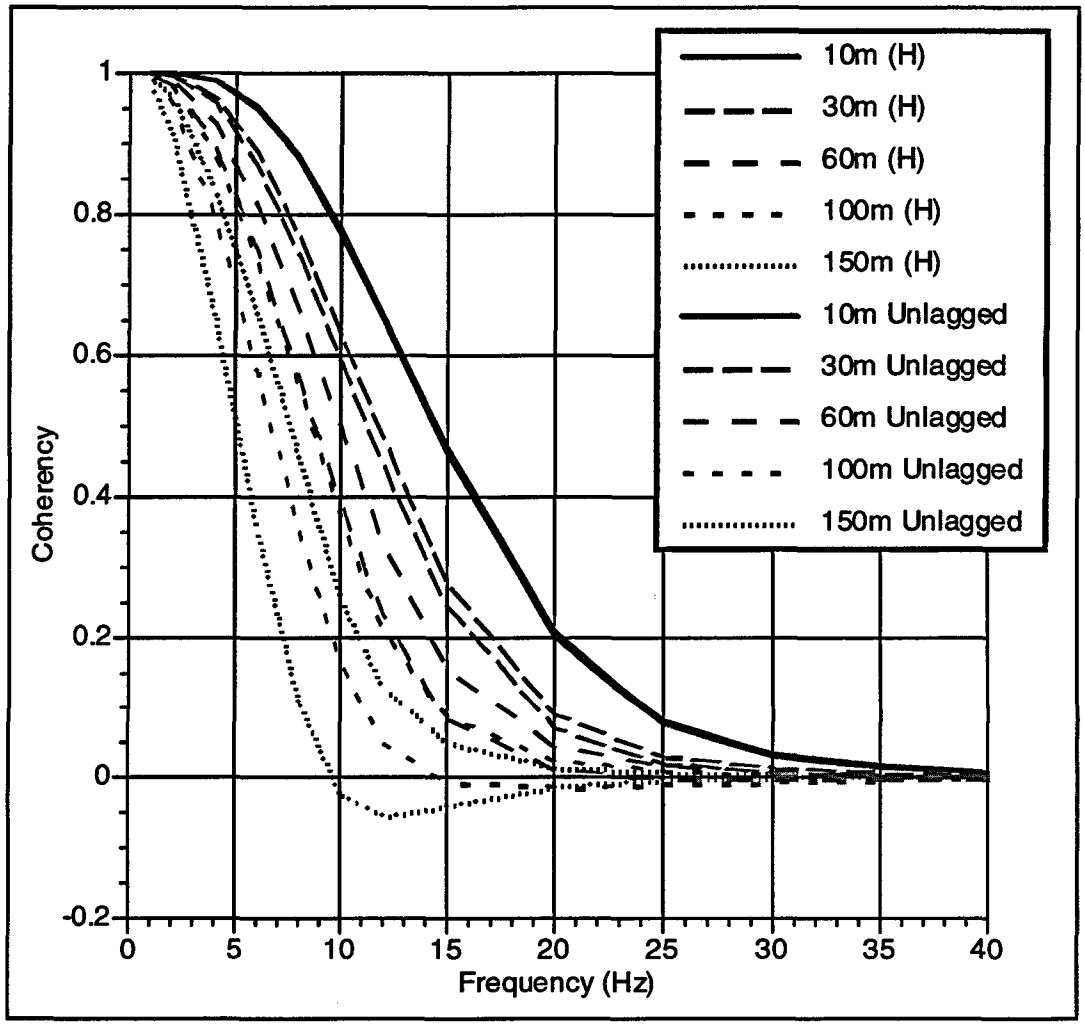

Figure 3-2
Comparison of the Unlagged Coherency (assuming an unknown direction of wave propagation) with the Plane-Wave Coherency for the Horizontal Component

The plane-wave coherency model is shown in Figure 3-1 for the horizontal and vertical components. Using a slowness of 0.25s/km (e.g. 4 km/s apparent velocity), the unlagged coherency for the modified model is compared to the plane-wave coherency in Figure 3-2. This shows the difference due to the wave-passage effect.

Evaluation of the Recommended Coherency Model

To evaluate the plane-wave coherency model given above requires that the relative timing of the recordings be available (including proper polarities). The two arrays with topographic effects were excluded from this analysis (USGS Parkfield and UCSC ZAYA). Two of the remaining arrays, Pinyon Flat and Stanford (temp) did not have reliable relative timing (this does not affect the lagged coherencies comparisons given in Abrahamson et. al. (1992). The plane-wave coherency residuals excluding the two arrays are shown in Figure 3-3. In this Figure, the mean residuals were computed for each array for separation distance bins of 0-15m, 15-30m, 30-60m, 60-100m, and 100-150m. This figure shows that the model is unbiased for the data sets considered.

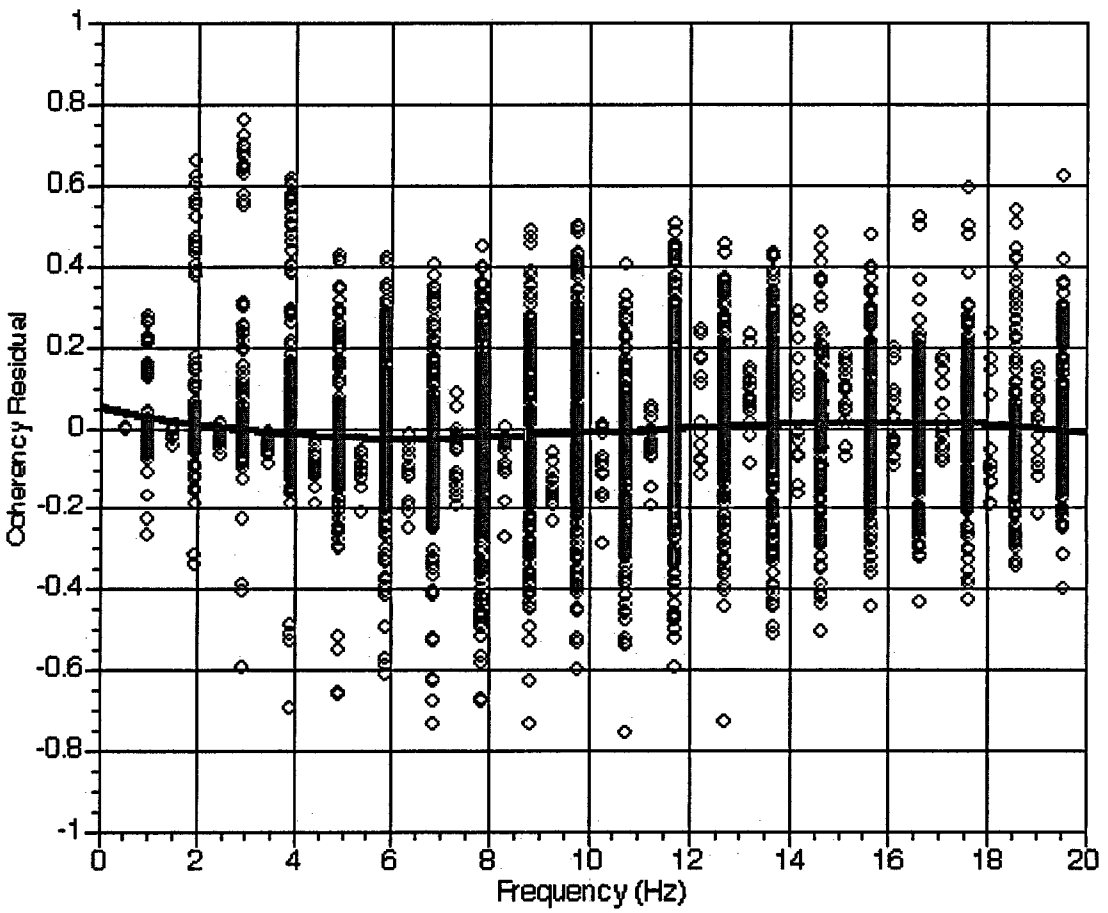

Figure 3-3
Residuals of Plane-Wave Coherency from 56 Earthquakes

The magnitude dependence of the plane-wave coherency residuals is shown in Figures 3-4 and 3-5 for frequencies of 5 Hz and 10 Hz, respectively. There is not a strong dependence for the larger magnitudes. At 10 Hz (Figure 3-5), the smaller magnitudes show a trend toward a positive residual indicating that they have slightly higher coherency than the larger magnitude earthquakes.

The site-to-source distance dependence of the plane-wave coherency residuals is shown in Figures 3-6 and 3-7 for frequencies of 5 Hz and 10 Hz, respectively. There is not a dependence on distance.

This comparison indicates that the proposed coherency model is generally applicable for SSI applications regardless of the site condition, earthquake magnitude, or distance as long as there are not significant topographic features at the site. For sites with strong topography, the coherency is expected to be lower.

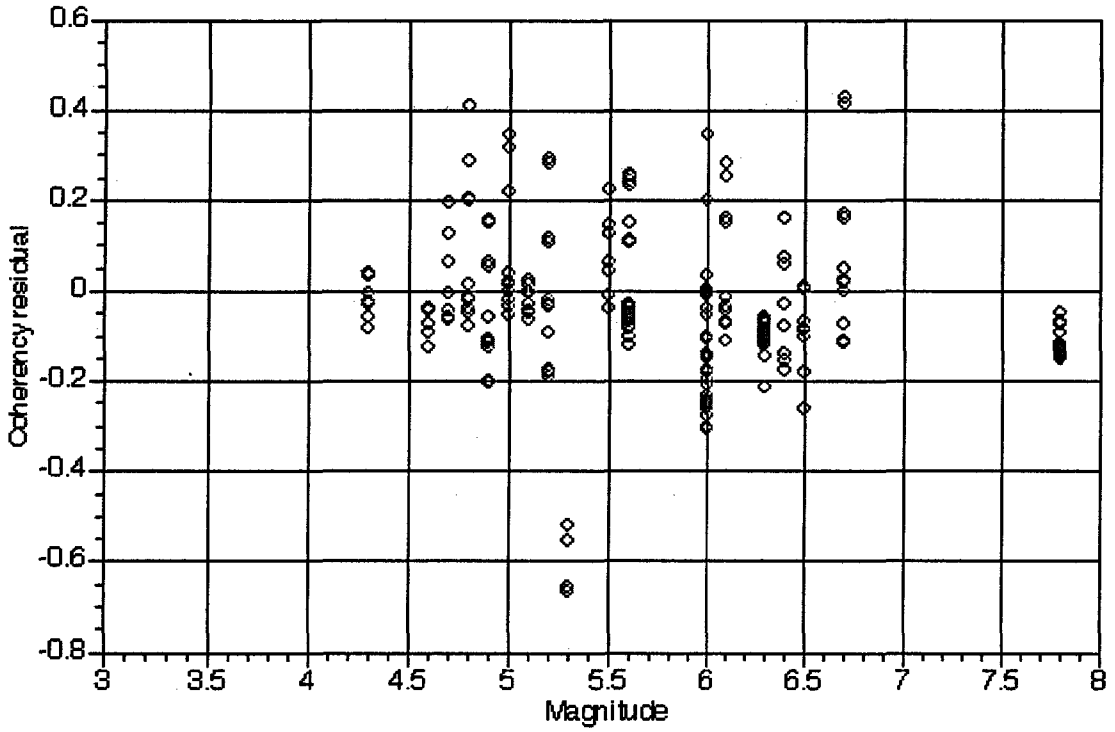

Figure 3-4
Plane-Wave Coherency Residuals at 5 Hz

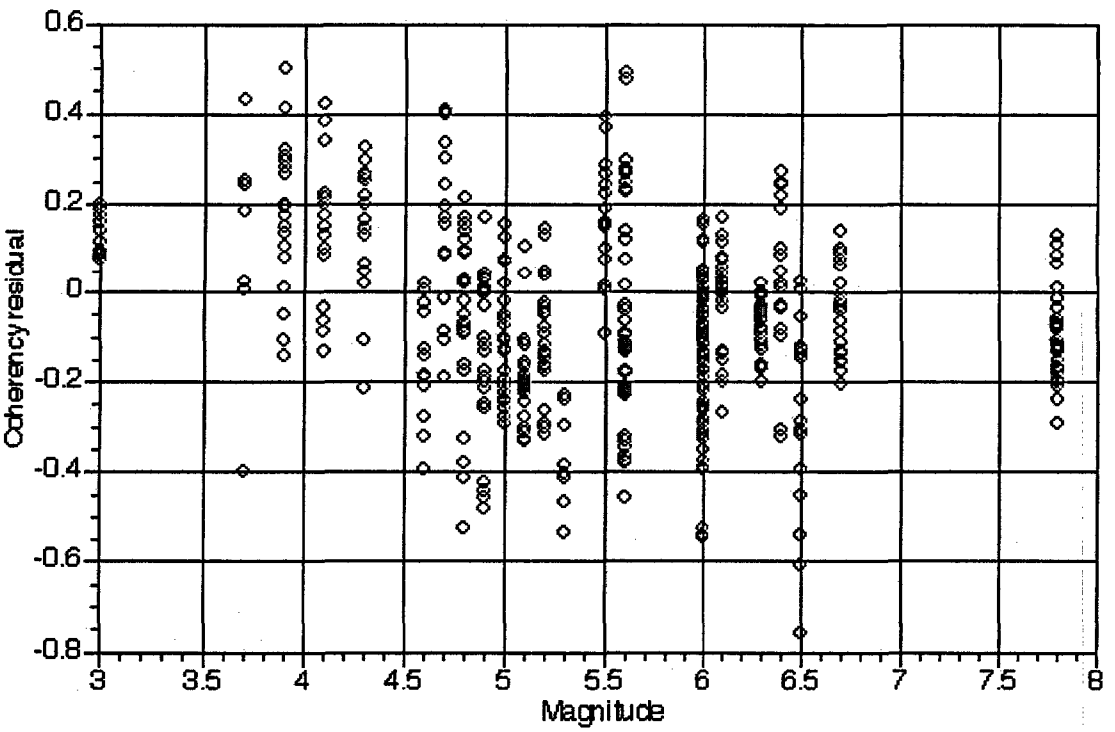

Figure 3-5
Plane-Wave Coherency Residuals at 10 Hz

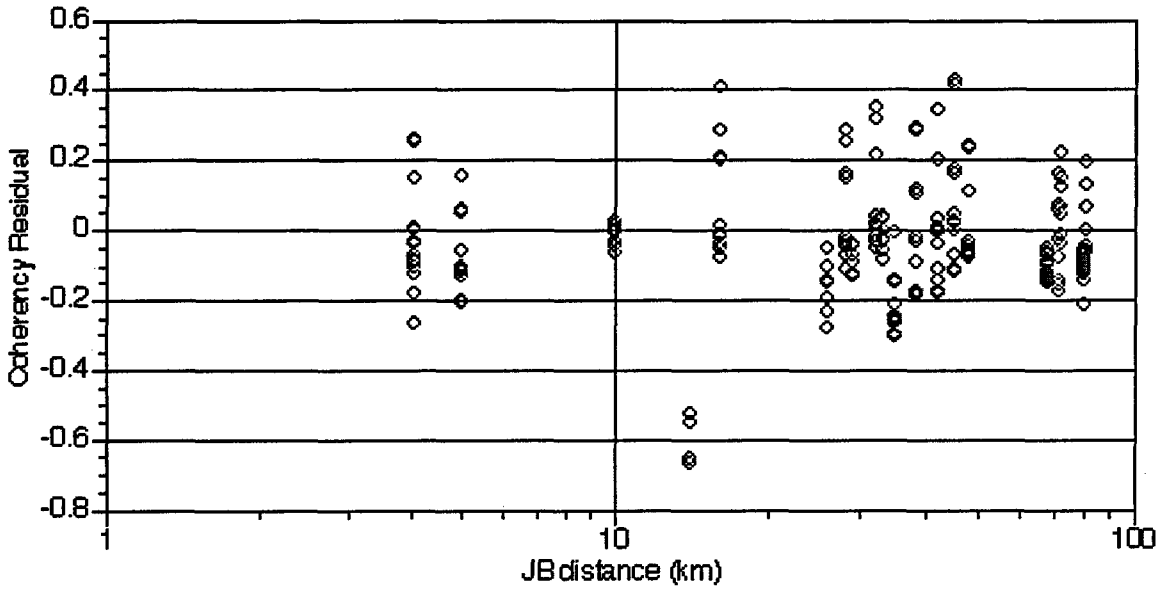

Figure 3-6
Plane-Wave Coherency Residuals at 5 Hz

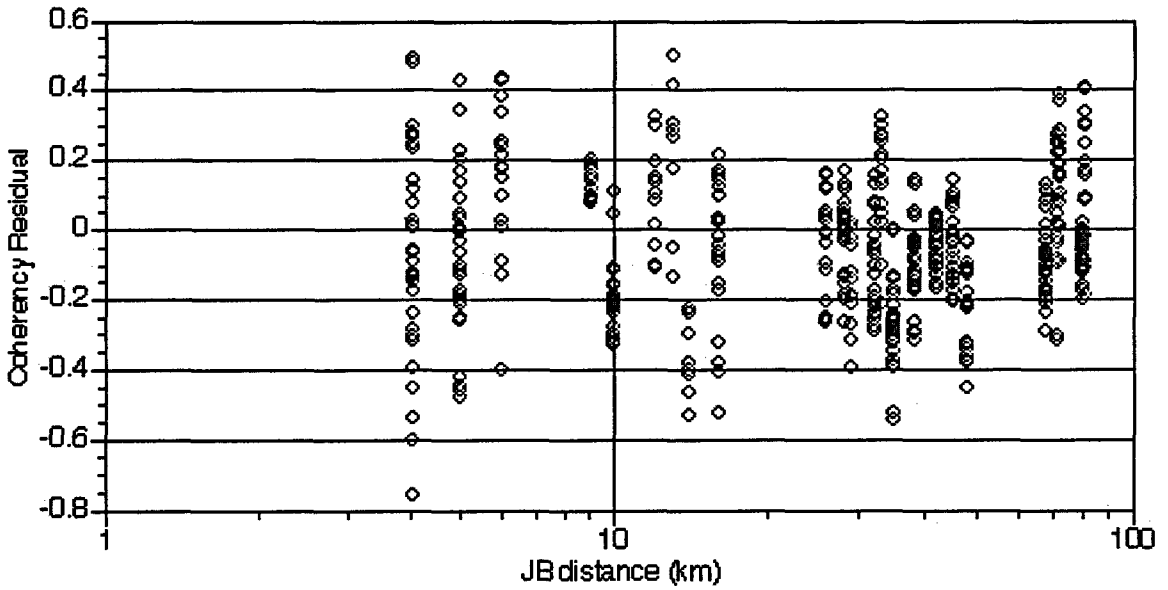

Figure 3-7
Plane-Wave Coherency Residuals at 10 Hz

4
CONCLUSIONS

Based on the comparisons with dense array data from a range of site conditions, earthquake magnitudes, and distances, the S-wave coherency models given in Tables 3-4 and 3-5 are considered to be generic and applicable to all site conditions except those with severe topography, and to all earthquake magnitudes and distances. While the models were only derived for frequencies up to 20 Hz, the extrapolation to higher frequency is considered to be reasonable because average coherency must continue to decrease as the frequency is increased until zero coherency is reached.

The coherency models were derived for the S-waves with window lengths of 2-10 seconds. For very high frequencies (e.g. > 10 Hz), it is possible that over very short time windows (e.g. 0.5 sec), the coherency at very high frequencies could be larger than the coherency for the full S-wave windows used here.

5
REFERENCES

Abrahamson, N. A., B. A. Bolt, R. B. Darrah, J. Penzien, and Y. B. Tsai (1987). The SMART-1 accelerograph array (1980-1987): A review, Earthquake Spectra, Vol. 3, pp. 263-287.

Abrahamson, N. A. and J. Schneider (1988). Spatial coherency of shear waves from the Lotung large-scale seismic experiment, Proceedings of the International Workshop on Spatial Variation of Earthquake Ground Motion, Princeton University, Dunwalke, New Jersey.

Abrahamson, N. A., J. F. Schneider, and J. C. Stepp (1991). Empirical spatial coherency functions for application to soil-structure interaction, Earthquake Spectra, Vol. 7, pp. 1-28.

Abrahamson, N. A., J. F. Schneider, and J. C. Stepp (1992). The spatial variation of earthquake ground motion and effect of local site conditions, Proceedings of the Tenth World Conference Earthquake Engineering, Madrid, Spain.

Abrahamson, N, A. (1993). Spatial variation of multiple support inputs, Proc. First US Seminar on Seismic Evaluation of Retrofit of Steel Bridges, A Caltrans and University of California at Berkeley Seminar, San Francisco, CA.

Abrahamson, N. A. (1998). Empirical plane-wave coherency models for horizontal and vertical components, Appendix F in "Seismic ground motions report for San Francisco-Oakland Bay Bridge East Span Seismic Safety Project", Report to Caltrans. December 24, 1998.

Enochson, L. D. and N. R. Goodman (1965). Gaussian approximations to the distribution of sample coherence, Tech Rep. AFFDL-TR-65-57, Wright-Patterson Air Force Base.

Harichandran, R. S. and E. Vanmarcke (1986). Stochastic variation of earthquake ground motion in space and time, Journal of Engineering Mechanics, ASCE, Vol. 112(2), pp. 154-174.

Harichandran, R. S. (1988). Local Spatial variation of earthquake ground motion, Earthquake Engineering and Soil Dynamics II – Recent Advances in Ground Motion Evaluation, J. L. Von Thun (ed.), American Society of Civil Engineers, New York, pp. 203-217.

Harichandran, R. S. (1991). Estimating the spatial variation of earthquake ground motion from dense array recordings, Structural Safety, Vol. 10, pp. 219-233.

Loh, C. H. (1985). Analysis of the spatial variation of seismic waves and ground movements from SMART-1 data, Earthquake Engineering and Structural Dynamics, Vol. 13, pp. 561-581.

Loh, C. H. and Y. T. Yeh (1988) Spatial variation and stochastic modeling of seismic differential ground movement, Earthquake Engineering and Structural Dynamics, Vol. 16, pp. 583-596.

Loh, C. H. and S. G. Lin (1990). Directionality and simulation in spatial variation of seismic waves, Engineering Structures, Vol. 12, pp. 134-143.

Novak, M. (1987). Discussion of Stochastic variation of earthquake ground motion in space and time by R. S. Harichandran and E. H. Vanmarcke, Journal of Engineering Mechanics, Vol. 113, pp. 1267-1270.

Oliveira, C. S., H. Hao, and J. Penzien (1991). Ground motion modeling for multiple-input structural analysis, Structural Safety, Vol. 10, pp. 79-93.

Ramadan, O. and M. Novak (1993). Coherency functions for spatially correlated seismic ground motions, Geotechnical Research Center Report No. GEOT-9-93, Univ. Western Ontario, London, Ontario, Canada.

Vernon, F. J. Fletcher, L. Carroll, A. Chave, and E. Sembera (1991). Coherence of seismic body waves as measured by a small aperature array, Journal of Geophysical Research, Vol. 96, pp. 11981-11996.

Zerva, A. and O. Zhang (1997). Correlation Patterns in Characteristics of Spatially Variable Seismic Ground Motions, Earthquake Engineering and Structural Dynamics, Vol. 26, pp. 19-39.

Zerva, A. and V. Zervas (2002). Spatial Variation of Seismic Ground Motions: An Overview, Journal of Applied Mechanics Reviews, ASME, Vol. 55, pp. 271-297.

Export Control Restrictions

Access to and use of EPRI Intellectual Property is granted with the specific understanding and requirement that responsibility for ensuring full compliance with all applicable U.S. and foreign export laws and regulations is being undertaken by you and your company. This includes an obligation to ensure that any individual receiving access hereunder who is not a U.S. citizen or permanent U.S. resident is permitted access under applicable U.S. and foreign export laws and regulations. In the event you are uncertain whether you or your company may lawfully obtain access to this EPRI Intellectual Property, you acknowledge that it is your obligation to consult with your company's legal counsel to determine whether this access is lawful. Although EPRI may make available on a case-by-case basis an informal assessment of the applicable U.S. export classification for specific EPRI Intellectual Property, you and your company acknowledge that this assessment is solely for informational purposes and not for reliance purposes. You and your company acknowledge that it is still the obligation of you and your company to make your own assessment of the applicable U.S. export classification and ensure compliance accordingly. You and your company understand and acknowledge your obligations to make a prompt report to EPRI and the appropriate authorities regarding any access to or use of EPRI Intellectual Property hereunder that may be in violation of applicable U.S. or foreign export laws or regulations.

The Electric Power Research Institute (EPRI)

The Electric Power Research Institute (EPRI), with major locations in Palo Alto, California, and Charlotte, North Carolina, was established in 1973 as an independent, nonprofit center for public interest energy and environmental research. EPRI brings together members, participants, the Institute's scientists and engineers, and other leading experts to work collaboratively on solutions to the challenges of electric power. These solutions span nearly every area of electricity generation, delivery, and use, including health, safety, and environment. EPRI's members represent over 90% of the electricity generated in the United States. International participation represents nearly 15% of EPRI's total research, development, and demonstration program.

Together...Shaping the Future of Electricity

Printed on recycled paper in the United States of America

1012968

ELECTRIC POWER RESEARCH INSTITUTE

3420 Hillview Avenue, Palo Alto, California 94304-1395 • PO Box 10412, Palo Alto, California 94303-0813 • USA
800.313.3774 • 650.855.2121 • askepri@epri.com • www.epri.com